



Mildred S. Dresselhaus

FUTURE DIRECTIONS IN CARBON SCIENCE

M. S. Dresselhaus

Department of Electrical Engineering and Computer Science, and Department of
Physics, Massachusetts Institute of Technology, Cambridge, Massachusetts 02139

KEY WORDS: graphite, diamond, carbon fibers, fullerenes, nanotubes

ABSTRACT

The materials science of carbon-based materials has enjoyed a tremendous growth in the past half century. Selected highlights are reviewed with emphasis given to future opportunities in this research field.

INTRODUCTION

The bulk phases of carbon have been studied since ancient times. One outstanding breakthrough that occurred in carbon science during my early scientific career was the synthesis of diamond in the laboratory under conditions of high temperature and pressure (1, 2). This development had a major impact on science by sparking excitement in new materials synthesis, and on technology by spawning the modern tool-and-dye industry and the diamond-coating industry. In the same year (1960), another important advance was made in carbon science, and though it had much less impact on the world of science and technology, the first synthesis of highly oriented pyrolytic graphite (HOPG) (3) had a large impact on my personal scientific career.

I started research in carbon science in 1961 and have participated in studying many aspects of carbon ever since. My earliest work in carbon science was a study on the electronic structure of graphite, using the magnetoreflexion technique, and it was the availability of the newly developed HOPG that provided a large enough sample with a long enough carrier mean free path ($\omega_c \tau \gg 1$) to allow such a measurement to be carried out. The success of this experiment led to a long series of further work over the next decade to elucidate the electronic

structure of graphite. For many years, especially in my early career, carbon science was a backwater field, considered by many to be too complicated and by others too mundane. I was always attracted to graphite and related materials because of their unique properties, the variety of behaviors they could exhibit under different circumstances, and the scientific and technical challenges in carrying out definitive experiments and in gaining understanding of the fundamental underlying science of this family of materials with extremes in properties. My students, coworkers, and I also enjoyed working in a field that was not in the limelight, where one could do careful work and take the time to understand what was going on. The unique properties exhibited by these materials provided wonderful thesis material and training ground in basic science for a generation of graduate students.

More recently, carbon science has gained high visibility with the discovery of fullerenes in 1985 (4) and carbon nanotubes in 1991 (5), and this visibility has been further heightened by the 1996 Nobel Prize in Chemistry award to Curl, Kroto & Smalley for their discovery of fullerenes. Although much attention has been focused on fullerenes and nanotubes, almost all aspects of carbon science have attracted increasing attention because of their relevance to fullerenes and nanotubes in some cases, but mostly because of their intrinsic interest now that many more researchers are familiar with the fundamentals of carbon science.

Because of my long experience with carbon materials, I have frequently been called upon to view the “big picture” of carbon science for both general audiences and for specialists working on either fullerenes or carbon nanotubes and put these recent “hot topics” in broad perspective. Although I have given many talks on aspects of this broad picture, I have never had an occasion to pull these pieces together to present them in written form, until the review presented here. Having settled on the topic of my prefatory article, I was then confronted with the selection of a proper format. In this regard, I have chosen to take a glimpse into my view of the future of this science field rather than to review past accomplishments, because I thought this format would allow me to write a more interesting and useful article that would stimulate both young people and experienced workers into rewarding future research opportunities in a field that has been so fascinating to me.

I would now like to return to the discussion of the carbon phase diagram (Figure 1) that guided the historical synthesis of diamond in 1960, noting that Francis Bundy, one of the coauthors of this 1996 rendition of the phase diagram (6), was himself a coauthor of the historical 1960 version (7, 8). Although we have learned much about the phases of carbon in the intervening 36 years, much ignorance remains about the phases of carbon, with many new directions awaiting exploration for this fundamental and universally common form of matter. From Figure 1, it is immediately seen that sp^2 -bonded graphite is

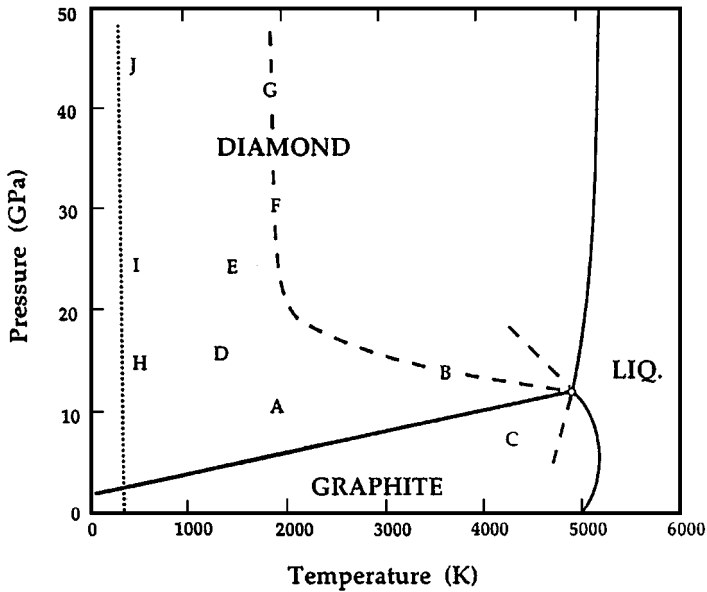


Figure 1 A recent version of the phase diagram of carbon (6) emphasizing graphite, cubic diamond, and hexagonal diamond phases, as well as liquid carbon. Solid lines represent equilibrium phase boundaries. A: commercial synthesis of diamond from graphite by catalysis; B: P/T threshold of very fast (<1 ms) solid-solid transformation of graphite to diamond; C: P/T threshold of very fast transformation of diamond to graphite; D: single crystal hexagonal graphite transforms to retrievable hexagonal-type diamond; E: upper ends of shock compression/quench cycles that convert hex-type graphite particles to hex-type diamond; F: upper ends of shock compression/quench cycles that convert hex-type graphite to cubic-type diamond; B, F, G: threshold of fast P/T cycles, however generated, that convert either graphite or hexagonal diamond into cubic-type diamond; H, I, J: path along which a single crystal hex-type graphite compressed in the c -direction at room temperature loses some graphite characteristics and acquires properties consistent with a diamond-like polytype, but reverts to graphite upon release of pressure.

the ground state phase under ambient conditions. At higher temperatures and pressures, a stability region for sp^3 -bonded cubic diamond is shown, whereas other regions show stability ranges for hexagonal diamond and the liquid phase. In addition, researchers have identified other bulk phases such as the hexagonal carbynes (9–16), and very recently the exotic carbolite phase has been reported (17, 18). However, not enough is known about these more exotic phases of carbon for inclusion in phase diagrams such as the one shown in Figure 1. Despite the significant effort that has already gone into studying the phase diagram of carbon, many researchers believe that a variety of novel carbon bulk phases are yet to be discovered and explored. Although this article is limited to

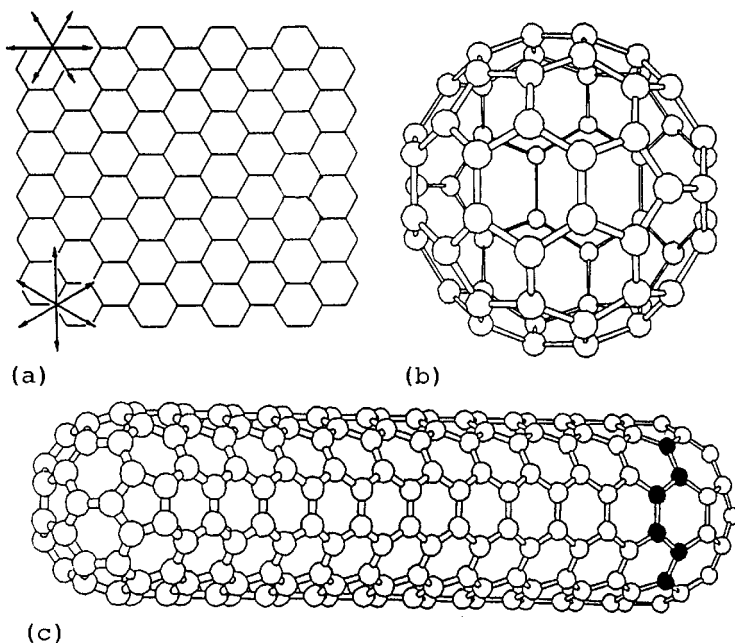


Figure 2 Stable forms of carbon clusters: (a) a piece of a graphene sheet, (b) the fullerene C_{60} , and (c) a model for a carbon nanotube.

research frontiers in sp^2 carbon, it should be noted that research in sp^3 carbon has been in an extremely active phase since the discovery of new synthesis routes for diamond films (19).

In addition to the bulk phases featured in the carbon phase diagram, a great deal of attention has been focused on small carbon clusters (20), since the discovery of fullerenes in 1985 by Kroto et al (4) and of carbon nanotubes in 1991 by Iijima (5). The physical reason why these nanostructures form is that a graphene layer (defined as a single layer of three-dimensional graphite) of finite size has many edge atoms with dangling bonds, and these dangling bonds correspond to high-energy states. Therefore, the total energy of a small number of carbon atoms (in the 30–100 range, as shown schematically in Figure 2a) is reduced by eliminating dangling bonds, even at the expense of an increase in strain energy, thereby promoting the formation of close cage fullerene molecules, the most stable being C_{60} (Figure 2b). A similar argument applies to the formation of carbon nanotubes (Figure 2c), which can be considered as quantum wires, analogous to considering fullerenes as quantum dots.

In this article, selected topics in carbon science are briefly reviewed in light of future research opportunities.

GRAPHITE-RELATED FRONTIERS

Although the properties of bulk graphite are by now well understood (21, 22), this field continues to attract attention both in research and in pedagogy. I have been significantly involved in the pedagogical activities during the past decade, serving as the Graffin Lecturer of the American Carbon Society in 1982. Because graphite remains the foundation for present research frontiers, there is much interest in its structure and properties for use in understanding the recently discovered forms of carbon. Thus work continues in an effort to refine our present understanding of graphite, and these efforts are further encouraged by the synthesis and preparation of improved graphite materials, by the development of more sensitive characterization methods, and by the introduction of more powerful computational capabilities. In this context, here we review highlights of recent studies and offer a glimpse on future opportunities in the study of carbon ribbons, doped graphene clusters, carbolite, and graphite intercalation compounds.

Graphene Ribbons

One topic that is attracting attention recently is the study of the electronic structure of graphene ribbons. Two examples of edge states are shown in Figure 3 for graphene ribbons terminated by armchair edges (Figure 3a) and by zigzag edges (Figure 3b). Many important commercial carbon materials, such as carbon fibers and glassy carbon, contain carbon networks that can be approximated by graphene ribbons (22). The recent finding that zigzag-terminated ribbons (Figure 3b) possess a unique edge state close to the Fermi

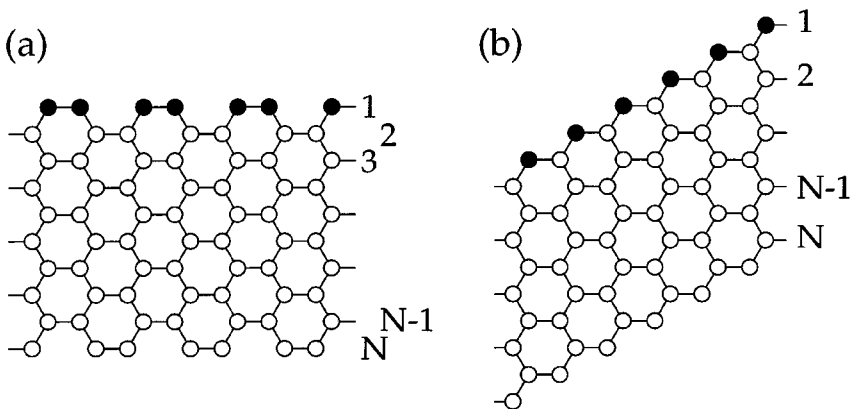


Figure 3 Graphene ribbons terminated by (a) armchair edges and (b) zigzag edges, indicated by filled circles. The indices denote the atomic rows for each ribbon. The model for the electronic structure considers hydrogen termination of the dangling bonds.

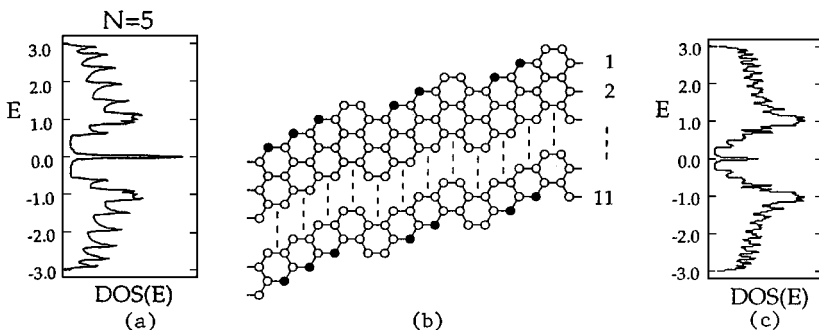


Figure 4 (a) The density of electronic states for a zigzag ribbon for $N=5$ (see Figure 3b). (b) The unit cell of a general graphene ribbon of $N=10$. The zigzag sites are indicated by filled circles. (c) The density of state [DOS(E)] corresponding to (b). The zigzag edge state is responsible for the sharp peak in the DOS at the Fermi level (23).

level (Figure 4a), not present for armchair-terminated ribbons (Figure 3a), has stimulated interest in the electronic structure of these graphene ribbons (22–24). If the ribbon size of a random ribbon is of narrow width and has a sufficient fraction of zigzag terminations (Figure 4b), this feature in the density of states persists (Figure 4c). This finding could perhaps have some impact on the tailoring of commercial carbons to possess certain desired properties, by controlling the graphene ribbon width. Studies of edge states could also have some relevance to the properties of porous carbons, which have a very high density of edge states.

Doped Graphene Clusters

Carbon has long been used for electrodes and for battery applications. Recently, carbon has been widely discussed as a host material for lithium in lithium-ion batteries (25, 26) (for more detail see below). The experimental finding that disordered carbons can take up Li to higher concentrations (by a factor of ~ 3) (25) than the stage 1 ordered graphite intercalation compound C_6Li (27) offers promise for enhanced battery performance relative to the graphite host material. This finding has fueled theoretical interest in the doping of disordered carbons, and I have been involved in stimulating such interests. Significant insight into the Li–C binding mechanism has been obtained by looking for the most active sites for lithium binding onto a graphene cluster (Figure 5), calculating the amount of charge transfer between the carbon cluster and the lithium ions, and determining the stability of various edge sites in comparison with the bulk sites that dominate lithium uptake in a crystalline graphite intercalation compound. Figure 5a shows a C_{96} graphene cluster to which a single Li atom (*shaded*)

is attached, with the optimal distances shown for the lithium atom from the surrounding carbon atoms at the edges for this particular binding site. Also given are the magnitudes and signs of the charges on the various neighboring sites. The charge transfer from the Li ion to the graphite cluster is located at the edge region. However, the ionicities of the two nearest-neighbor carbon atoms are almost zero. When the dangling bonds on the cluster are terminated by hydrogen atoms, different sites are favored for Li uptake, as shown in Figure 5*b*. For example, weak bonding to an out-of-plane site for Li attachment is found, in this case (Figure 5*b*), where the amount of charge transfer is also indicated using the same notation as in Figure 5*a*. In time, more sophisticated models for doped carbon clusters will become available.

Carbolites

Carbolites were recently discovered (17) in an effort to prepare larger quantities of previously discovered carbynes for detailed measurements. Carbynes are a condensed form of carbon featuring chain-like carbon-carbon sp^1 bonding. Carbynes have been identified in two stable phases (labeled α and β) (9, 14), and both phases are hexagonal, with lattice constants: $a_\alpha = 8.94 \text{ \AA}$, $c_\alpha = 15.36 \text{ \AA}$; and $a_\beta = 8.24 \text{ \AA}$, $c_\beta = 7.68 \text{ \AA}$ (15). Application of pressure converts the α phase into the β phase. The numbers of atoms per unit cell and the densities are, respectively, 144 and 2.68 g/cm^3 for the α phase, and 72 and 3.13 g/cm^3 for the β phase (29). Carbynes have been identified in some meteorites, but relatively little is known about them. There are thus wide-open research opportunities available in the study of carbynes, as soon as improved synthesis routes are established.

Carbolite is a newly discovered chain-like crystalline form of carbon that was first synthesized in 1995 in a carbon arc and, because of its relatively low mass density ($\rho_m = 1.46 \text{ g/cm}^3$), is called carbolite (17). Depending on whether hydrogen is contained with argon as the ambient gas in the arc, two distinct crystal structures have been obtained and identified by analysis of X-ray diffraction patterns. Type I carbolites are synthesized in argon gas and have a hexagonal crystal structure with $a_0 = 11.928 \text{ \AA}$, $c_0 = 10.62 \text{ \AA}$, whereas type II carbolites with lattice constants $a_0 = 11.66 \text{ \AA}$, $c_0 = 15.68 \text{ \AA}$ are formed using an argon-hydrogen gas mixture. These structures are presented schematically in Figure 6 for the two types of carbolites, showing the stacking of the four-atom carbon chains, with a nearest-neighbor distance of 1.328 and 1.307 \AA in the chain direction, and with a 3.443 and 3.366 \AA separation between the chains for type I and type II carbolites, respectively. In the type I structure, the four-atom chains have an AB stacking, whereas the type II structure shows ABC stacking. The nearest-neighbor C–C distance along the chains is close to that of graphite in-plane (1.42 \AA), and the interchain distances in Figure 6 are close to the

interlayer separation in graphite (3.35 Å). The complementarity of the carbolite structure to that of graphite attracted my interest to this exotic material. Infrared spectra suggest that the interchain bonding is of the $\text{-C}\equiv\text{C-C}\equiv\text{C-}$ polyene type. The electrical resistivity of undoped carbolites is very high and decreases upon intercalation with K, Na, and I_2 , with a six order of magnitude decrease in resistivity reported for K intercalation. The intriguing crystal structure in relation to graphite, and the recent report of superconductivity in K-doped carbolites (17, 18), have kindled interest in this esoteric carbon phase.

Graphite Intercalation Compounds

Graphite intercalation compounds (GICs) are formed by the insertion of layers of guest species between the layers of the graphite host material (27, 30), as shown schematically in Figure 7. Either atomic or molecular guest species may be inserted between the graphene layers because of the weak van der Waals interlayer forces associated with the sp^2 bonding in graphite. In donor GICs, electrons are transferred from the donor intercalate species (such as a layer of the alkali metal potassium) into the graphite layers, thereby raising the Fermi level E_F in the graphitic electronic states. The increase in E_F results in an increase in the mobile electron concentration by two or three orders of magnitude, while leaving the intercalate layer positively charged with low mobility carriers. Conversely, for acceptor GICs, electrons are transferred to the intercalate species (which is usually molecular) from the graphite layers, thereby lowering the Fermi level E_F in the graphitic electronic states and creating an equal number of positively charged hole states in the graphitic π -band. Electrical conduction in GICs (whether they are donors or acceptors) occurs predominantly in the graphene layers, and the enhanced conduction is a result of the large amount of charge transfer between the intercalate and host layers. The electrical conductivity between adjacent graphene layers is very poor (especially in the acceptor compounds, where the graphene layer separation is generally larger). The role of the intercalate species in modifying the properties of the host graphite material and the use of intercalation compounds to study low-dimensional physics have fascinated me and are the reasons why I have put so much effort into working in this area (27).

←

Figure 5 (a) An optimized Li geometry in the C_{96} cluster in which a $\text{Li}^{+0.29}$ ion is mostly covalently bonded to the two nearest-neighbor carbon atoms. (b) An optimized Li geometry in the hydrogen-terminated $\text{LiC}_{96}\text{H}_{24}$ cluster. Lithium intercalation can occur at hydrogen-terminated edges as well as edges containing no hydrogen atoms. In the insets we show the Li position from the top view, and an enlargement of the area near the Li ion is shown from the side view. We show also the ionicities of the Li and neighboring carbon atoms for which the absolute values are more than $0.03e$ (28).

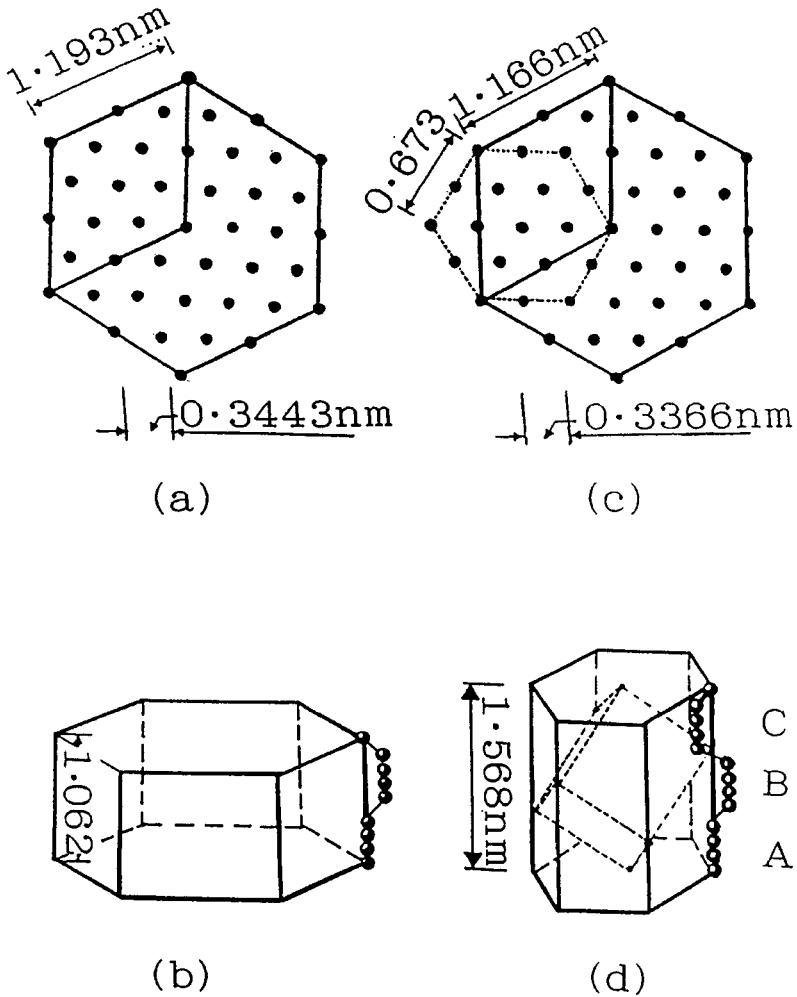


Figure 6 Structural model for the two forms of hexagonal carbolite. Hexagonal face (*top view*) of a unit cell showing alignment of the chains for (a) type I carbolite and (c) for type II carbolite. View of the four-atom carbon chains (b) with AB stacking for type I and (d) with ABC stacking for type II carbolite (17).

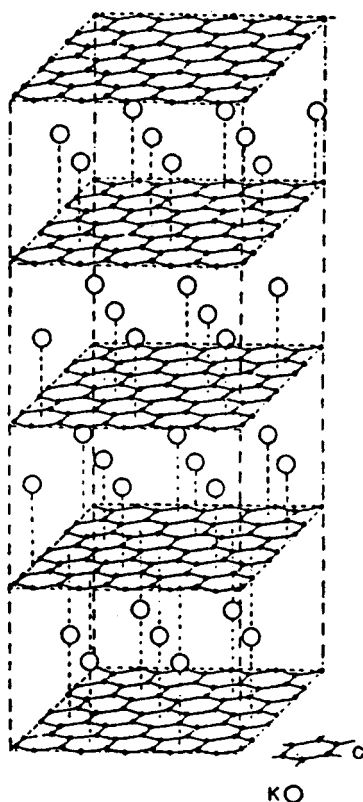


Figure 7 Schematic model for a graphite intercalation compound showing the stacking of graphite layers (networks of hexagons on a sheet) and of intercalate (e.g. potassium) layers (networks of large hollow balls). For this stage 1 compound, each carbon layer is separated by an intercalate layer (31).

Because of the competing attractive electrostatic interaction between the intercalate and the adjacent graphene layers and the repulsive interplanar interaction resulting from the intercalation-induced lattice strain, the intercalate layers form an ordered superlattice structure, interleaved with the graphite layers, through a phenomenon called staging (27, 30). A GIC of stage n has isolated intercalate layers separated from one another by n graphite layers, forming a unit cell along the c -axis normal to the layer planes of length

$$I_c = d_s + (n - 1)c_0, \quad 1.$$

in which d_s is the separation between the two graphite layers between which the intercalate is sandwiched.

Interest in the intercalation process has been rekindled by the observation of intercalation in fullerene-based crystalline phases, in carbon nanotubes, and in carbolites. The charge transfer process observed for the doping of fullerenes by alkali metals and alkaline earths is similar to that occurring in donor graphite intercalation compounds. Such doping transfers electrons to fullerenes, thus forming fullerene anions. Also, the distances of the dopants to the nearest-neighbor carbon atoms are similar for doped fullerenes and for GICs. However, the conduction process in doped fullerenes is very different from that in GICs because of differences in electronic bandwidths and in the dimensionality of the conduction process. Because of the high electro-negativity of fullerenes, charge transfer in fullerenes occurs commonly for donor compounds, but acceptor fullerene compounds do not form except in a few special cases (20). Less is known about the characteristics of the intercalation process in carbon nanotubes and in carbolites, as compared with graphite, which has been studied for many years.

Although the study of GICs is generally considered to be a mature research field, the general high level of activity in carbon science research at present has also stimulated GIC research. One branch is along traditional directions of new intercalate species and further refinement of structure/property relations in GICs. The new research areas include development of thin film host materials for intercalation based on new precursors such as polyimides (32–36) and the study of intercalation in novel carbon forms such as disordered carbons, fullerene-based crystalline phases, carbon nanotubes, carbolites, and carbon nanoparticles.

FULLERENES

Fullerenes, first discovered in 1985 by Kroto et al (4) in an attempt to explain anomalous infrared and ultraviolet carbon spectra from outer space, have received much attention in the past decade, especially since the announcement by Krätschmer & Huffman in 1990 (37) of a synthesis method capable of producing gram quantities of fullerenes, thereby opening the field to numerous investigators, including my own research group (20). By now the basic structure of C_{60} (see Figure 2*b*) and many of its physical properties are understood (20), although many refinements and the development of applications still can be expected. Some of the many areas identified as open research opportunities are further discussed in this section. Because of the high symmetry of C_{60} , its relatively high abundance, and the fact that all C_{60} molecules are identical (except for the isotope effects), C_{60} is a prototype nanostructure for modeling purposes.

Although progress has been made in modeling fullerene growth, the growth mechanism is not yet well understood (38), and no report has been published

about the growth of fullerenes from the constituent clusters corannulene and pyracylene. Many research opportunities remain for finding inexpensive methods for growing the fullerenes C_{60} and C_{70} . The availability of copious amounts of these fullerenes is expected to spur on the development of applications. Similarly, research on the growth of single-phase higher mass fullerenes ($n_C > 70$ in C_{n_C}) should be encouraged, including the separation of fullerenes of a given mass into their constituent isomers. Because of the interesting symmetries that can occur in these isomers, study of the structure and properties of specific isomer species presents both difficult challenges but rewarding outcomes if successful synthesis and purification routes are found.

Among the various physical properties of fullerenes, the transport properties are among the least well understood. Since most of the work to date has been done on fullerene-derived crystals that had been exposed to oxygen, and because oxygen adsorption can change the measured conductivity by several orders of magnitude (39–41), there is a need for improved transport measurements, especially for undoped fullerenes. Further understanding of conduction mechanisms, especially regarding the energetics of the photoconductivity process, is needed, and issues related to the reason why metallic conductivity is limited to a narrow range of stoichiometry ($x \simeq 3$) in M_xC_{60} remain to be clarified (20).

Whereas fullerenes generally form highly molecular solids with narrow bands and wide bandgaps, irradiation by ultraviolet light, the application of pressure, or the doping with alkali-metals M to the composition MC_{60} all serve to couple fullerene molecules to form oligomers, and in some cases polymerized solid phases of MC_{60} compounds are formed. Figure 8 shows the joining of two C_{60} molecules to form a dimer (42). While early work was directed toward suppressing polymerization, more recent work has focused on characterizing the structure and properties of the polymerized phases, developing models for the intermolecular bonding, and seeking applications such as masks and patterning (43) that utilize these polymerized phases. These oligomers or polymer phases are presently under intensive study. The formation of oligomers was first identified through characteristic changes in the Raman spectra due to the lowering of the icosahedral symmetry (42). Raman spectroscopy has thus become an excellent method for the characterization of oligomer formation (44). The optical spectra of fullerenes have unique features arising from the fact that the optical transitions from the valence and conduction bands are symmetry forbidden, so that the transitions observed at the absorption edge are phonon assisted and can be studied to some degree through electron spectroscopy techniques. Because the phonon-assisted transitions are weak, early studies have used rather high photon intensities, which often resulted in photo-degradation of the fullerene films. Thus many of the nonlinear optics studies on fullerenes need to be revisited (45).

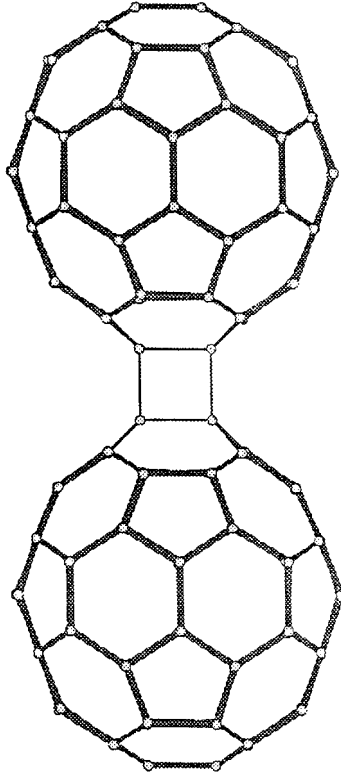


Figure 8 Schematic model for a fullerene dimer.

However, from the standpoint of device applications, the special properties of the forbidden transitions give rise to increased absorption from excited states, so that fullerenes perform very well as an optical limiter, which is a device whose absorption increases as the incident light intensity increases, thereby protecting delicate optical instruments from over-exposure to photon irradiation.

A major applications area for fullerenes is expected to relate to chemical derivatives tailored for specific properties and applications. The use of small quantities of fullerenes to enhance the photo-sensitivity of selected polymers has been studied for practical applications. Although it is premature to identify specific applications areas that will become important, it is generally thought that the synthesis of tailored fullerene-derived materials will yield significant applications in the future, as discussed by Taylor & Walton (46).

The interaction between fullerene molecules and surfaces is another area considered for potential applications. Fullerenes bind strongly to metals and

to semiconductors with a high density of surface states, but bind much less strongly to each other or to surfaces having few dangling bonds, such as oxide surfaces or hydrogen-terminated surfaces. The strong bonding of C_{60} to metal surfaces and the weak C_{60} - C_{60} bonding greatly facilitates the preparation of C_{60} monolayers on a metal surface by depositing a multilayer of C_{60} on that surface and subsequently desorbing (at $\sim 300^\circ\text{C}$) all C_{60} layers except the one that strongly adheres to the surface. At a metallic surface, charge transfer occurs to make fullerene anions, allowing both positional and orientational alignment of the fullerene molecules to occur. The strong adhesion of C_{60} to Si because of its high density of dangling bonds and surface states, and the weak adhesion of C_{60} to the oxide SiO_2 , make it possible to replicate a patterned Si/ SiO_2 interface with C_{60} sticking to Si and not to SiO_2 . Such a patterned surface has been shown by Hamza to yield a patterned SiC interface when the patterned C_{60} /Si surface is suitably heat treated (47).

Techniques have been developed for manipulating fullerenes on conducting substrates using an STM tip or by use of a time-varying electric field to roll the molecules (48, 49). Progress with the manipulation of fullerenes on surfaces is expected to have an impact on a number of other fields of science that are dependent on the manipulation of structures on a nanometer scale.

Endohedral Fullerenes

Closely associated with fullerene molecules are endohedral fullerenes $M_n@C_{n_c}$, consisting of a fullerene shell C_{n_c} into which a dopant species M_n has been added (see Figure 9) (20, 50). Most often M_n is a metallic species, in which case the endohedral fullerene is called a metallofullerene. Thus far, only a very small quantity of purified endohedral fullerene material is available. However, good progress is being made in the synthesis and purification of endohedral fullerenes with regard to their mass, and some success has already been achieved in the separation of specific isomers for a given molecular mass C_{n_c} (50). Isomers refer to the collection of fullerenes with the same number of carbon atoms n_c , but with pentagons and hexagons arranged in different physical structures, often with different point group symmetries. The availability of larger amounts of well-characterized uniphase endohedrally doped fullerene materials (with regard to both n_c and isomer) is expected to open up a new research area with promise for both interesting science and applications.

Alkali metal dopants have special interest because they can serve as either endohedral or exohedral dopants. Calculations of the ionization energies for $\text{K}_2@C_{60}$ (54) were used to determine the location of the alkali metal atoms (ions) within the C_{60} cage. Calculations of the charge transfer for many endohedral dopants into C_{60} have already been carried out, including the donors K, Ca, Mn, Sr, Ba, La, Eu, and U, and the presumed acceptors O and F (55).

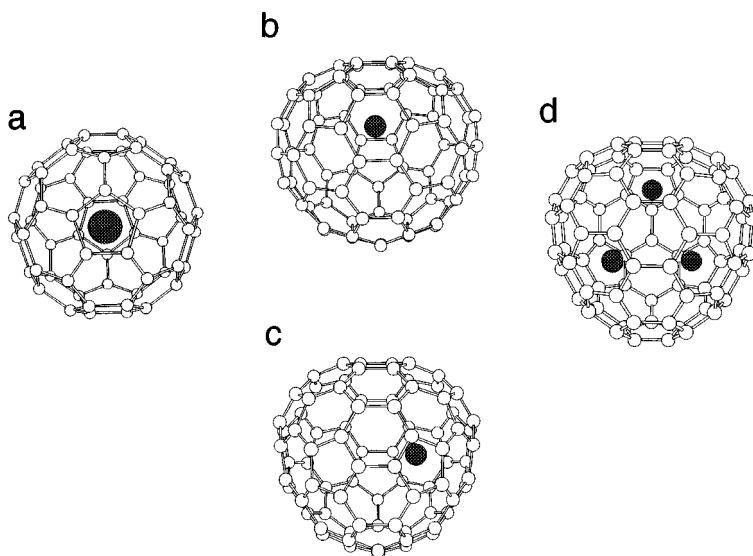


Figure 9 Structural models for various endohedral fullerenes. (a) Structural model for $\text{La}@C_{60}$, with La at the center of the C_{60} cage (51). (b, c) Structural models for $\text{La}@C_{82}$, with the La at two different off-center positions within the C_{82} cage (52). (d) Structural model for $\text{Sc}_3@C_{82}$ (assuming C_{3v} symmetry of the C_{82} cage), where black circles represent the three equivalent Sc^{3+} ions, which rapidly reorient within the C_{82} cage (53).

Metal-Coated Fullerenes

Not only is it possible to insert metal species within fullerenes, but it is also possible to coat fullerenes with alkali metals or alkaline earths (56). Whereas only one layer of alkali metal (e.g. Li) atoms has thus far been placed around a fullerene, they have been coated with multiple metal layers (up to four) using alkaline earth atoms such as Ca. For example, a lithium atom over the center of each pentagonal face of C_{60} (57, 58) produces $\text{Li}_{12}C_{60}$, in agreement with the observed stoichiometry. Mass spectra show peaks corresponding to $C_{60}M_{32}$, $C_{60}M_{104}$, $C_{60}M_{236}$, and $C_{60}M_{448}$, which can be explained by the models shown in Figure 10. In the case of the alkaline earth coatings, the metal atoms position themselves over the centers of all polygons, not only the pentagons, as is the case with the alkali metal coatings. The layers for the alkaline earth metal coatings can be described using the notation adopted for endohedral metallofullerenes, with $C_{60}@M_{32}@M_{72}@M_{132}@M_{212}$ describing the five concentric shells of the metal-coated cluster.

Future research opportunities on metal-coated fullerenes include exploration of new structures that may form either with alkali metal or alkaline earth metal

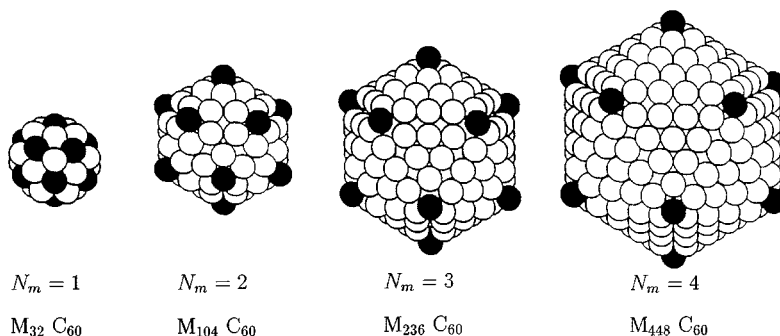


Figure 10 Proposed arrangements in multilayer metal-covered fullerenes of the atoms $M = Ca$ in the first four layers surrounding a C_{60} molecule. The M atoms over the icosahedral vertices of C_{60} are represented by black circles (56).

coatings, or with other metal species such as transition metals. The physical properties of fullerenes within a conducting shell, a magnetic shell, and a superconducting shell should lead to interesting research topics. Theoretical calculations investigating the stability of metal-coated particles as a function of numbers of layers, the location of the metal species within a shell, and the dependence of the physical properties on the identity of the metal species will be helpful for supporting an experimental program in this area.

CARBON NANOTUBES

Carbon nanotube research is probably the most active research field in carbon science. The first identification in 1991 of carbon nanotubes and their relation to fullerenes (5) attracted attention to the field, stimulating a large number of theoretical works on the structure and properties of single-wall carbon nanotubes one atomic layer in thickness, although all early experimental work was done on multi-wall carbon nanotubes. The experimental discovery of single-wall carbon nanotubes in 1993 (59, 60) further stimulated work in the field, though only small amounts of the single-wall nanotubes were available. In addition, the single-wall nanotubes were generally found along with very much larger concentrations of carbon nanoparticles and other carbon-based materials. Even within the single-wall nanotube segment of the sample, the nanotubes generally showed a distribution of diameters and geometries as explained below. For these reasons most of the experimental studies continued to be done on the multi-wall nanotubes. The discovery in 1996 of a much more efficient synthesis route, involving laser vaporization of graphite (61) to prepare arrays of ordered single-wall nanotubes, offers major new opportunities for quantitative

experimental studies of carbon nanotubes and is expected to have a large impact on the field.

Carbon nanotubes relate to fullerenes insofar as nanotubes are capped at either end by half of a fullerene, so that the smallest diameter nanotube corresponds to the smallest diameter fullerene (C_{60}), which has a diameter of 7.1 Å. Whereas small diameter carbon fibers (~ 70 Å diameter) had been produced as far back as 1975 (62, 63) and had been observed in TEM by many groups in the 1980s (including my own group at MIT), the connection between the nanotubes and fullerenes was not made until 1991 (20). My own interest in the nanotubes stems from extensive experience with carbon fibers (22), going back to 1980 when my collaborative research with Professor Morinobu Endo on carbon fibers started. More specifically, my interest has focused on the opportunities to study one-dimensional physics made possible by these new materials.

The fundamental carbon nanotube is a single-wall structure with three basic geometries—armchair, zigzag, and chiral—as shown schematically in Figure 11. The structure of the nanotube can be understood by referring to Figure 12, which demonstrates the rolling of a segment of a single graphite layer (called a graphene sheet) into a cylinder. In this figure we see that points O and A are crystallographically equivalent on a graphene sheet. The points O and A can be connected by a chiral vector $\vec{C}_h = n\hat{a}_1 + m\hat{a}_2$, where \hat{a}_1 and \hat{a}_2 are unit vectors for the honeycomb lattice of the graphene sheet. Next we draw normals to \vec{C}_h at points O and A to obtain lines OB and AB' . If we now superimpose OB onto AB' , we obtain a cylinder of carbon atoms that constitutes a carbon nanotube when properly capped at both ends with half of a fullerene. In accordance with this discussion, a single-wall carbon nanotube is uniquely determined by the integers (n, m) . From an experimental standpoint, it is more convenient to denote each carbon nanotube by its diameter $d_t = |\vec{C}_h|/\pi$ and the chiral angle θ , which \vec{C}_h makes with the zigzag direction ($\theta = 0$), as shown in Figure 12. The relation between the integers (n, m) and the characterization parameters d_t and θ are

$$d_t = C_h/\pi = \sqrt{3}a_{C-C}(m^2 + mn + n^2)^{1/2}/\pi, \quad 2.$$

where a_{C-C} is the nearest neighbor C–C distance, C_h is the length of the chiral vector C_h , and the chiral angle θ is given by

$$\theta = \tan^{-1}[\sqrt{3}m/(m + 2n)]. \quad 3.$$

The zigzag nanotubes $(0, 9)$ and $(9, 0)$ are equivalent because of the sixfold symmetry of the graphene layer. For example, a zigzag nanotube ($\theta = 0^\circ$) specified by $(9, 0)$ has a theoretical nanotube diameter of $d_t = 9\sqrt{3}a_{C-C}/\pi = 7.05$ Å, whereas an armchair nanotube specified by $(5, 5)$ has $d_t = 15a_{C-C}/\pi =$

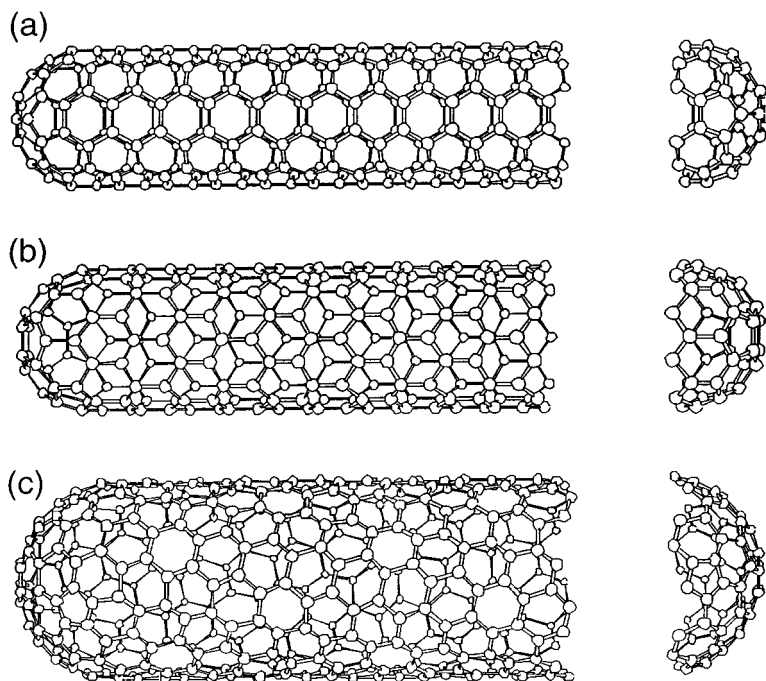


Figure 11 Schematic models for single-wall carbon nanotubes with the nanotube axis normal to (a) the $\theta = 30^\circ$ direction (an armchair (n, n) nanotube); (b) the $\theta = 0^\circ$ direction (a zigzag $(n, 0)$ nanotube); and (c) a general direction \overline{OB} (see Figure 12) with $0 < \theta < 30^\circ$ [a chiral (n, m) nanotube]. The actual nanotubes shown in the figure correspond to (n, m) values of (a) $(5, 5)$; (b) $(9, 0)$; and (c) $(10, 5)$ (64).

6.83 Å, both derived from hemispherical caps for the C_{60} molecule and assuming an average $a_{C-C} = 1.43$ Å appropriate for C_{60} .

Single-wall carbon nanotubes are interesting examples of a one-dimensional periodic structure along the axis of the nanotube. Confinement in the radial direction is provided by the monolayer thickness of the nanotubes. In the circumferential direction, periodic boundary conditions apply to the enlarged unit cell that is formed in real space and the subsequent zone folding that occurs in reciprocal space. We can then expect to observe one-dimensional dispersion relations for electrons and phonons in C_{60} -derived nanotubes. The unit cell of the one-dimensional carbon nanotube is a rectangle formed by the vectors \vec{C}_h and \vec{T} shown in Figure 12, where \vec{T} is the smallest lattice vector from O in the direction normal to \vec{C}_h . Because the basis vectors \vec{C}_h and \vec{T} of the one-dimensional unit cell are large compared with those of the unit cell for the graphene sheet,

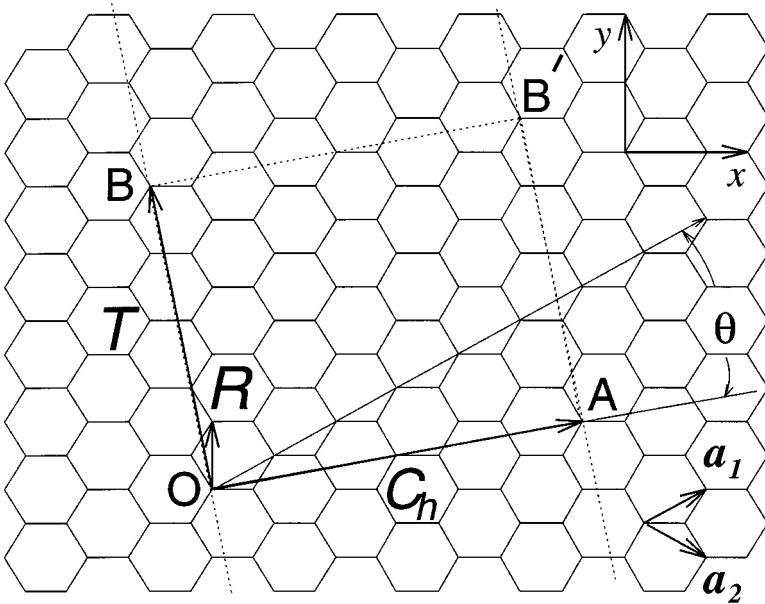


Figure 12 The chiral vector \vec{OA} or $\vec{C}_h = n\hat{a}_1 + m\hat{a}_2$ is defined on the honeycomb lattice of carbon atoms by unit vectors \hat{a}_1 and \hat{a}_2 and the chiral angle θ with respect to the zigzag axis, $\theta = 0^\circ$. Also shown is the lattice vector $\vec{OB} = \vec{T}$ of the one-dimensional nanotube unit cell. The rotation angle ψ and the translation τ (not shown) constitute the basic symmetry operation $R = (\psi | \tau)$ for the carbon nanotube. The diagram is constructed for $(n, m) = (4, 2)$. The area defined by the rectangle $(OAB'B)$ is the area of the one-dimensional unit cell of the nanotube.

the reciprocal space unit cell (Brillouin zone) is small compared with the bulk. Therefore, zone folding of the dispersion relations for a graphene sheet into the Brillouin zone for the one-dimensional nanotube is expected to give a first approximation for the dispersion relations for a carbon nanotube.

Calculation of these dispersion relations shows remarkable electronic properties, namely that for small-diameter graphene nanotubes, about one third of the nanotubes are metallic and two thirds are semiconducting, depending on the fiber diameter d_f and chiral angle θ . Metallic conduction in a carbon nanotube is achieved when

$$2n + m = 3q, \quad 4.$$

where n and m are integers specifying the nanotube diameter and chiral angle, and q is an integer. Nanotubes satisfying Equation 4 are indicated in Figure 13 as points surrounded by circles and these are the metallic nanotubes. The closed circles in this figure correspond to semiconducting nanotubes.

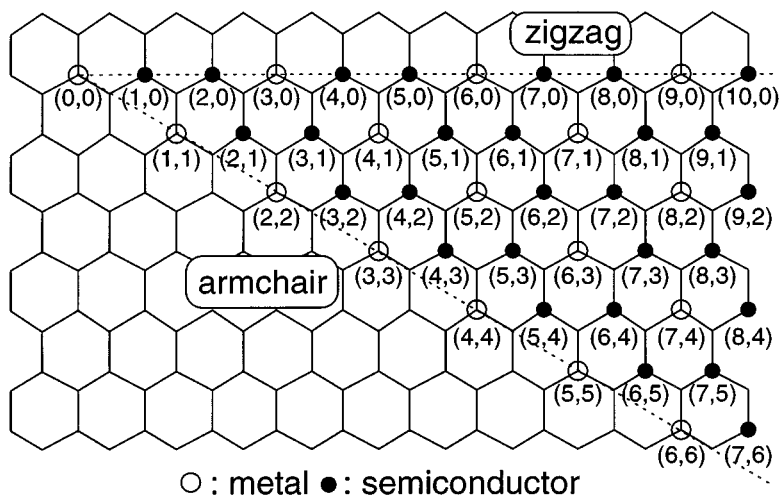


Figure 13 Chiral vectors (n, m) for carbon nanotubes showing metallic (*open circles*) and semiconducting (*closed circles*) behavior.

The calculations show that all armchair (n, n) nanotubes are metallic, but only one third of the possible zigzag nanotubes are metallic (65), which is also true for the chiral nanotubes. It may seem surprising that the calculated electronic structure can be either metallic or semiconducting depending on the choice of (n, m) , although there is no difference in the local chemical bonding between the carbon atoms in the nanotubes, and no doping impurities are present (65). These surprising results can be understood on the basis of the electronic structure of two-dimensional graphite, which is a zero gap semiconductor (66) with bonding and antibonding π bands degenerate at the K -point (zone corner) of the hexagonal Brillouin zone. The periodic boundary conditions permit only a few wave vectors to exist in the circumferential direction. If one of these wave vectors passes through the K -point in the Brillouin zone where the valence and conduction bands of two-dimensional graphite are degenerate, then metallic conduction results.

Several experiments have been carried out to test the theoretical predictions for the electronic properties of carbon nanotubes. Scanning tunneling microscopy/spectroscopy (STM/STS) studies (67) confirm that some nanotubes are metallic and some are semiconducting and show that the bandgap for the semiconducting nanotubes varies as the reciprocal of the nanotube diameter, independent of nanotube chirality, in agreement with theoretical calculations (20). Recent experiments of the resistivity of ropes of single-wall armchair carbon nanotubes (61) confirm the theoretical prediction that armchair nanotubes are metallic.

The recent breakthrough in the synthesis of single-wall carbon nanotubes is expected to greatly increase their availability and to strongly stimulate a wide variety of property measurements. The large increase in yield ($>70\%$) and the availability of ordered nanotube arrays (in a two-dimensional triangular lattice) in which almost all of the nanotubes have the armchair (n, n) structure with $n \sim 10$ (corresponding to an average reported diameter of 1.38 ± 0.002 nm) should provide an abundance of samples that can be used to obtain quantitative information about the one-dimensional quantum aspects of carbon nanotubes. These quantum effects are expected to be present in the electronic structure, lattice modes, Raman and infrared spectra, transport properties, and mechanical properties of single-wall carbon nanotubes. These remarkable properties suggest opportunities of future nanotube applications, perhaps in composites with other materials.

There remain excellent research opportunities for exploration of the growth mechanism of the nanotubes and refinements on present synthesis routes to provide more controlled growth of nanotubes with the same diameter d_t and chiral angle θ . Many opportunities exist for the development of sensitive characterization techniques for objects 1 nm in size and for the controlled manipulation of the nanotubes. Advances made in the characterization and manipulation of nanotubes should have a substantial impact on the science and technology of nanometer structures more generally. Progress that has been made in understanding the structure and properties of the junction region between two dissimilar carbon nanotubes (68–71) is encouraging and should stimulate further experimental and theoretical work.

CARBON NANOPARTICLES

Many of the same synthesis methods used in the synthesis of fullerenes and carbon nanotubes, such as arc discharge and laser vaporization, can be used to prepare hollow nanoparticles or filled nanocapsules. The filled nanocapsules are synthesized when the carbon electrode or carbon target is fabricated from a mixture of carbon with a small amount of an appropriate transition metal or rare earth metal. The carbon coating may consist of a few nanometers of disordered carbon or of polygonized graphene shells (see Figure 14) and serves to passivate the core material, which is often reactive. Likewise, the core of the nanoparticle is either fully filled or partially filled with a crystalline or disordered form of the transition metal or rare earth metal that was previously introduced into the carbon electrode or carbon target. The shape of the carbon structure that is formed depends critically on the growth conditions. These nanoparticles have recently become an active research area in terms of the development of improved synthesis routes, as well as structural, magnetic, and

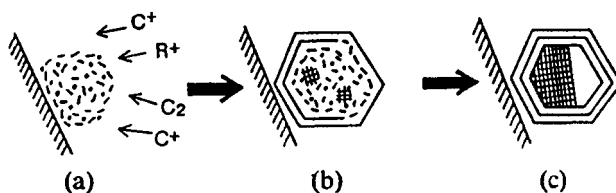


Figure 14 A growth model of a nanocapsule partially filled with a crystallite of rare earth metal carbide (RC_2 for $R = Y, La, \dots, Lu$; R_3C_4 for $R = Sc$) using an arc method: (a) R-C alloy particles, which may be in a liquid or quasi-liquid phase, are formed on the surface of the cathode; (b) solidification (graphitization) begins from the surface of the particle, and R-enriched liquid is left inside; (c) the graphite cage (*outside*) equilibrates with the metal carbide (*inside*) (72).

superconductivity studies of filled carbon nanoparticles, and the development of a host of practical applications such as magnetic inks. The higher melting point rare earth metals or metal-carbides tend to form partially filled nanocapsules (see Figure 14), whereas the transition metals are more likely to form filled capsules.

An example of a carbon-coated nanoparticle (30–70 nm diameter) (73) with the morphology of Figure 14 is the YC_2 nanoparticle. These particles show faceted graphitic faces with an average turbostratic interlayer distance of 0.344 nm, containing crystalline YC_2 with lattice spacings corresponding to the (002) plane, and a void volume or cavity in addition to the single-crystal YC_2 material. This is consistent with initial crystallization of the graphitic shell, i.e. the Y-C alloy remains molten while the graphitic shell crystallizes. When the YC_2 composition is reached, there is a crystallization of the YC_2 (73).

Hollow concentric carbon spheres are also formed upon intense electron beam irradiation of carbon nanoparticles with faceted shapes (74–76) (see Figure 15). Of particular interest is the recent finding of an innermost sphere with an inner diameter of 7.1 Å, corresponding to the diameter of the C_{60} molecule. It is found that if enough energy is provided, the formation of concentric spherical shell structures is favored over the coaxial nanotube structures for small numbers of carbon atoms (74, 75). Using these techniques, spherical shells with diameters up to 100 Å have been synthesized (see Figure 15), with dimensions similar to those reported for spherical shells of small-sized carbon blacks. Although containing a large amount of strain energy, the spherical shells have no dangling bonds and are stable under further electron bombardment, even when containing only a few (2–4) spherical shells (77, 78). Ugarte has speculated that the concentric spherical shells (or onions as they are often called) constitute another form of carbon, consisting of a fullerene at the center and epitaxial, concentric layers of carbon shells about the central core

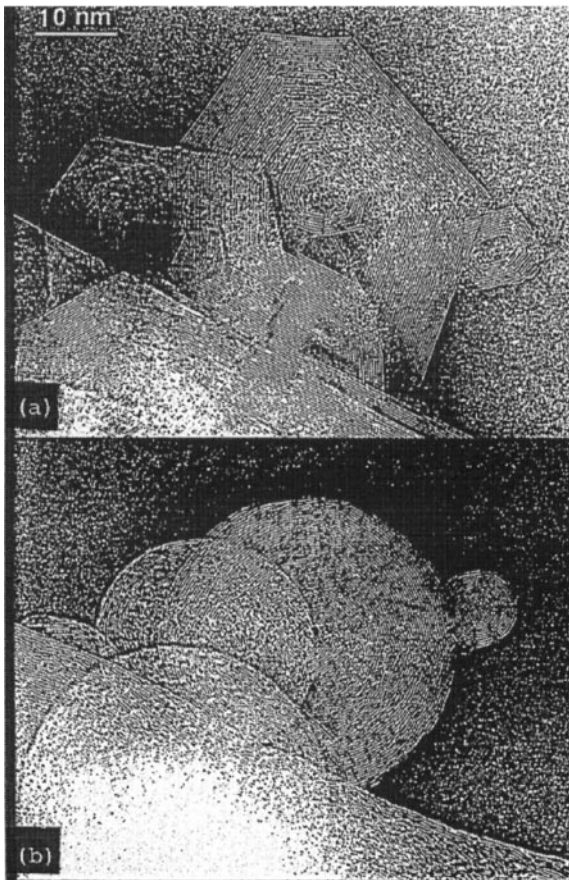


Figure 15 High-resolution electron micrographs of graphitic particles: (a) As obtained from an electric arc deposit, the particles display a well-defined faceted structure and a large inner hollow space and (b) the same particles after being subjected to intense electron irradiation. The particles now show a spherical shape and a much smaller central empty space (76).

(74, 75). Onion-like multilayer carbon shells can also be generated by shock wave treatment of carbon soot (79), from carbon deposits exposed to a plasma torch (80), by laser melting of carbon within a high-pressure (50–300 kbar) cell (81), and by annealing nanodiamonds at temperatures in the range 1100 to 1500°C (82).

The growth of carbon layers is believed to begin at the surface and progress toward the center (75, 83). The onion-like carbon particles are stabilized by the energy gain from the weak van der Waals interaction between adjacent carbon

shells (78, 84, 85). The size (number of carbon atoms) at which the total energy of a closed surface particle becomes equal to a planar graphite sheet remains unanswered both theoretically and experimentally. The synthesis and purification of macroscopic quantities of quasispherical onion-like particles with a small-size distribution remain major challenges to studying the properties of carbon onions.

DISORDERED CARBONS

After spending much of my early career studying the electronic structure of ideal sp^2 -bonded carbon, I later became interested in disordered carbons, which exhibit more general sp , sp^2 , and sp^3 bonding. This new interest developed in the following way. In 1980, I became aware of the work of Professor Morinobu Endo in Japan on the synthesis of vapor-grown carbon fibers that could be prepared with resistivity values ($55 \mu\Omega\text{cm}$) only slightly higher than those for single-crystal graphite flakes ($40 \mu\Omega\text{cm}$). These fibers provided an excellent host material for the study of the transport properties of graphite and its intercalation compounds. In trying to understand the defects commonly found in the vapor-grown carbon fibers, I was drawn into a new area of carbon science dealing with disordered carbons. This was and remains an area of great technological importance, where the research is done largely in industry and is more product oriented than fundamental, and where relatively few systematic studies have been carried out thus far. Even today, the study of disordered carbon systems offers many opportunities for fundamental and systematic research in areas such as glassy carbons, carbon fibers, activated carbons, porous carbons, ion-implanted carbons, and others.

Disordered carbons are frequently characterized (22) by their in-plane crystallite size (L_a), which is conveniently studied by Raman spectroscopy (86); the c -axis crystallite size (L_c), which is determined by X-ray diffraction; and the interlayer spacing d_{002} , which is also obtained from X-ray diffraction measurements. Figure 16 shows a schematic model for the structure of a carbon fiber, where long graphene ribbons are stacked parallel to one another to achieve L_c values on the order of tens of nanometers, although there is little site correlation in the stacking of the carbon atoms on adjacent layers. This type of stacking is called turbostratic stacking. In ideal single-crystal graphite with perfect Bernal interlayer AB stacking, the interlayer spacing is $d_{002} = 3.35 \text{ \AA}$. The introduction of disorder increases d_{002} , and when site correlation disappears and turbostratic stacking is established, we find that $d_{002} = 3.44 \text{ \AA}$, as shown in Figure 17. As d_{002} increases, the physical properties exhibit more two-dimensional behavior. In the following sections, several examples of disordered carbons, which are attracting my personal attention, are discussed.

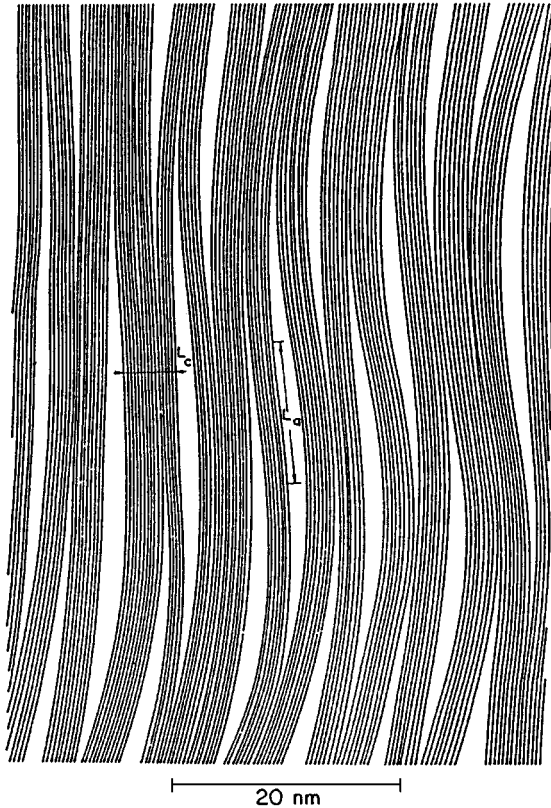


Figure 16 Sketch of the cross section of a PAN fiber along the fiber axis direction (87). Here the in-plane and c -axis structural coherence lengths L_a and L_c are indicated (22).

CARBON FIBERS

Most commercial carbon fibers exploit the great strength of these materials under tension, which is best achieved when the carbon fibers are prepared from a polymer precursor such as polyacrylonitrile (PAN), whereas fibers prepared from a mesophase pitch liquid crystal precursor are used for high modulus (stiffness) applications. The tensile strength of steel is 1.4 Gpa; that for a PAN fiber can be five times greater. Likewise, the modulus of steel is 207 Gpa, whereas pitch fibers have moduli more than four times greater.

A major emphasis of research and development in carbon fibers is in the development of a cheaper and better synthesis route to promote the use of

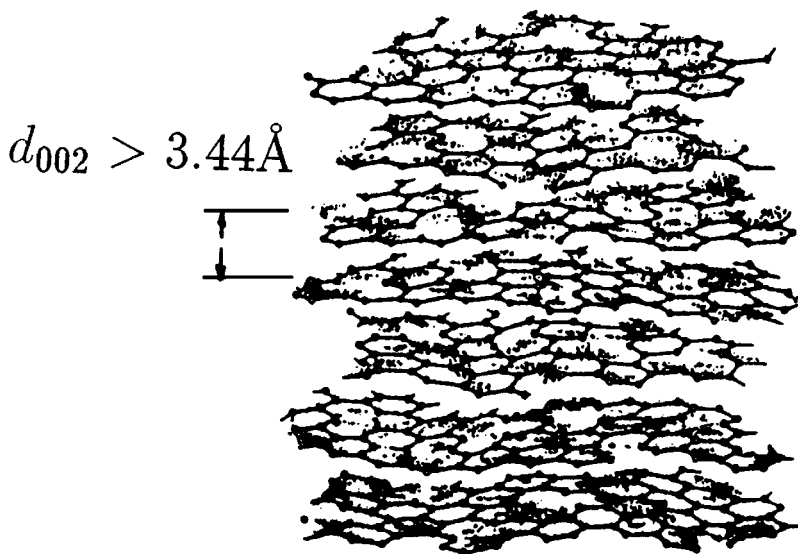


Figure 17 Schematic presentation of the turbostratic stacking of graphene planes in carbons. The loss of interlayer correlation leads to an increase in the interlayer separation, denoted by d_{002} in the figure, to values in excess of 3.44 Å (22, 88).

this unique class of materials. Once the cost of carbon fibers becomes more competitive with other structural materials, the demand for carbon fibers will increase, particularly for fibers with specially tailored microstructures. The demonstration of fiber alignment by use of a magnetic field (89) could be helpful for aligning chopped fibers for specific applications.

Recent demonstrations that both vapor-grown carbon fibers and multi-wall carbon nanotubes originate from a single-wall carbon nanotube (see Figure 18) (90, 91) have stimulated interest in comparative studies between vapor-grown carbon fibers and carbon nanotubes in the hope of further advancing carbon fiber synthesis techniques or the use of carbon nanotubes for niche applications, where they could surpass carbon fibers in performance. Of course, the cost of carbon nanotubes would have to be greatly reduced for carbon nanotubes to be of commercial interest.

CARBON FOR BATTERY APPLICATIONS

In experiments under ambient conditions, graphite can only accommodate lithium atoms up to the stoichiometry of the graphite intercalation compound LiC_6 (92). Through the introduction of dopants in graphitic systems (93), or the

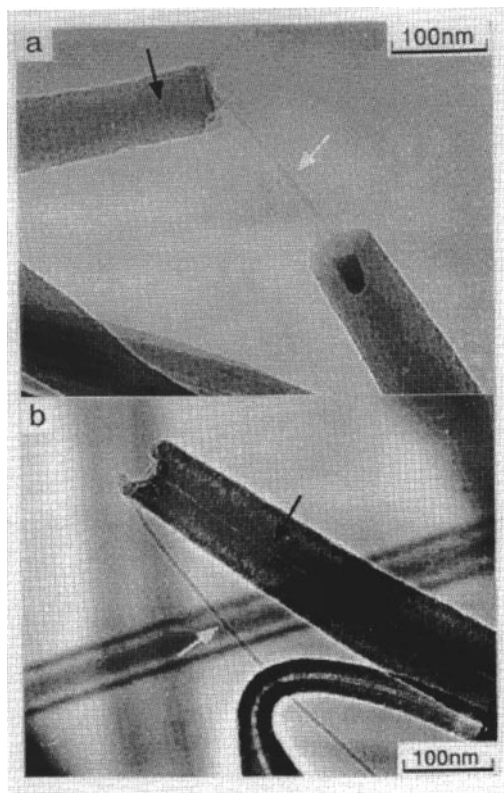


Figure 18 TEM picture of the broken portion of an as-grown nanofiber cross section. The nanotube core is exposed (91).

application of high pressures (94), larger amounts of Li may be accommodated into these carbon structures. This has created a great amount of interest in the practical application LiC_x systems that may be used as active anode materials in Li ion batteries with enhanced cell capacities (25, 95). It has been recently shown that some disordered carbons such as polyparaphenylene (PPP)-based carbons, prepared at relatively low heat treatment temperatures (T_{HT}), can accommodate very large amounts of lithium with Li:C ratios close to 1:2 (25). The characterization of the PPP host material over the heat treatment temperature range $650 < T_{\text{HT}} < 2700^\circ\text{C}$ shows the evolution of PPP from a partially dehydrogenated polymeric structure at $T_{\text{HT}} = 650^\circ\text{C}$ to a disordered graphitic structure for $T_{\text{HT}} = 2700^\circ\text{C}$. Of particular interest is the special nature of the structure of the PPP-based material near $T_{\text{HT}} = 700^\circ\text{C}$, where the highest Li

uptake has previously been reported (25). Both the Raman spectra (95) and the EPR spectra (97) indicate that the PPP host material evolves most rapidly from its polymeric structure to a disordered carbon for T_{HT} near 700°C . The ability of PPP heat-treated to $\sim 700^{\circ}\text{C}$ to accommodate enhanced amounts of Li may be linked both to structural features and to the existence of hydrogen-rich regions that provide electronically favorable sites for the binding of Li atoms or ions. Thus Li may localize not only within carbonized regions between weakly correlated graphene ribbons, as for a well-ordered GIC, but also within the uncarbonized regions that contain a mixture of hydrogenated graphene ribbons and disordered PPP. This would be consistent with the observation of two types of Li localization centers within the PPP heat-treated to 700°C . Cluster calculations for the most stable locations for Li on a graphene cluster (with or without hydrogenization) have been especially helpful to our group for gaining an understanding of the mechanism for Li uptake.

Many research opportunities are presently available in the simulation of the structure and properties for specific disordered carbons.

POROUS CARBONS, ACTIVATED CARBONS, AND AEROGELS

Among the exceptional properties of sp^2 -bonded carbons is their ability to form porous materials with very high surface area ($1000\text{--}3000\text{ m}^2/\text{g}$). Porous activated carbon materials (see Figure 19a) are generally synthesized through reaction with O_2 , H_2O , and/or CO_2 in the temperature range $800 < T < 1200^{\circ}\text{C}$ for pitch-based carbon fibers. One attraction of the activated carbon fibers over other porous carbon host materials is the relatively small pore size ($< 2\text{ nm}$) and the relatively narrow size distribution of these nanopores. Current emphasis

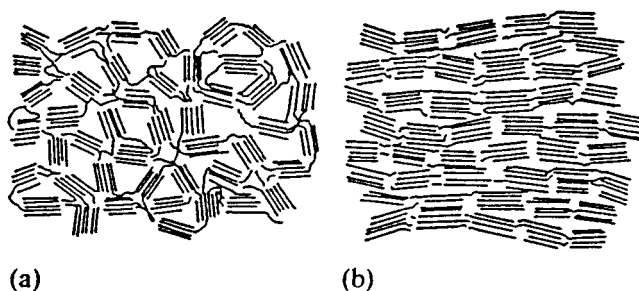


Figure 19 Schematic model for the microstructure of activated carbon fibers: (a) for a high surface area fiber where the basic structural units are randomly arranged and (b) for a fiber after some heat treatment, showing partial alignment of the basic structural units (98).

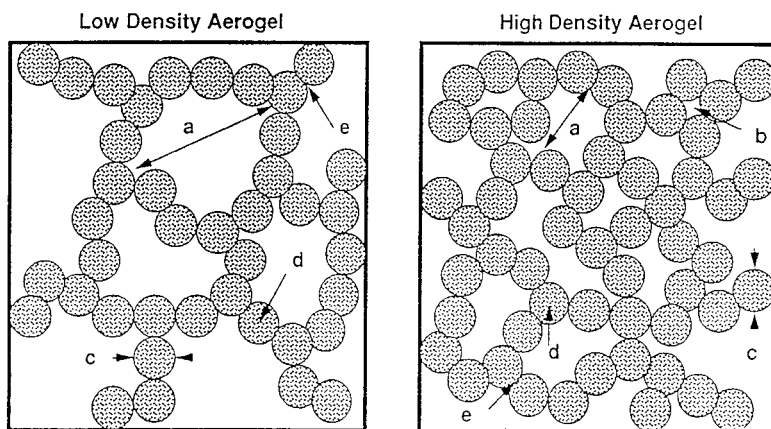


Figure 20 Schematic diagram of the carbon aerogel microstructure. Each shaded circle represents a disordered carbon particle. The microstructure is shown for (*left*) low ($\sim 0.1 \text{ g/cm}^3$) and (*right*) high ($\sim 0.6 \text{ g/cm}^3$) bulk density forms of carbon aerogels. The microstructure shows (*a*) mesopores that span the distance between chains of interconnected particles, (*b*) micropores sandwiched between particles, (*c*) individual particles ($\sim 12 \text{ nm}$ diameter), (*d*) micropores within the particles, and (*e*) micropores between contiguous particles (100).

is on the study of the pore structures and improved synthesis routes for the preparation of cheaper porous carbons with enhanced performance in terms of control of pore size and pore size distribution. Scientific systematic studies have used heat treatment (Figure 19*b*) and temperature-dependent measurements to gain insights into the structure and properties of these materials and the mechanisms controlling these properties.

Carbon aerogels are a disordered form of sp^2 -bonded carbon with an especially low bulk density and are synthesized by a supercooling process (99). These materials are examples of a class of cluster-assembled low-density porous materials, consisting of interconnected carbon particles with diameters typically near 12 nm (99, 100). Within each particle, a glassy carbon-like nanostructure is observed, consisting of an intertwined network of narrow graphitic ribbons of width $\sim 2.5 \text{ nm}$. The morphology is illustrated schematically in Figure 20 for both a low-density material ($\sim 0.1 \text{ g/cm}^3$) and a higher-density material ($\sim 0.6 \text{ g/cm}^3$) (100). This morphology leads to high surface areas ($600\text{--}800 \text{ m}^2/\text{g}$), with a wide distribution of pore diameters. For a given specific surface area, carbon aerogels tend to have larger size pores and a larger distribution of pore sizes than the activated carbon fibers discussed above. Because of their large surface areas and consequently high density of dangling bonds, porous carbons tend to have somewhat different electronic properties from those of other

disordered carbons. Activation of this carbon aerogel leads to very lightweight materials with surface areas comparable to those in activated carbon fibers. Thus far there has been very little reported work on the structure and properties of activated carbon aerogels.

A number of significant opportunities have been identified for carbon aerogel applications, including gas adsorption devices, separators for heavy metals and ions, purification of drinking water, and electronic capacitors. Current research activities focus on gaining a better understanding of the pore structure and its properties, initiating systematic studies of the structure and properties of activated carbon aerogels with surface areas up to perhaps 3000 m²/g. The science and technology of carbon aerogels would attract a lot more attention than it now does if cheaper synthesis routes could be found for the production of larger quantities of carbon aerogel material with enhanced and controlled properties.

CONCLUDING REMARKS

In viewing carbon science from a broad perspective, several overriding conclusions emerge. Various breakthroughs have had a large impact in bringing new workers into the field of carbon science, and the enlarged talent base drawn from their diverse science backgrounds has been crucial for the major advances that have been made. In almost every area, it was those breakthroughs that created new carbon materials that have been especially influential. While some of the big discoveries were motivated by desires for materials with specific properties, others with enormous impact, such as fullerenes and carbon nanotubes, arose from curiosity-driven research. Progress in the field has strongly benefited from close coupling between experiment and theory, going back to the 1950s when experimental and theoretical investigations at the Union Carbide Corporation Research Laboratory had a tremendous influence on the development of carbon fibers, quite independent of the activity already mentioned at the General Electric Research Laboratory in the laboratory synthesis of diamond. A more recent example of this productive synergy occurred at the NEC Research Laboratory in Tsukuba, Japan in the area of fullerenes and carbon nanotubes.

At present, there is much activity both in diamond-related *sp*³ carbon and graphite-related *sp*² carbon research. Although most workers devote their attention to one or the other of these subfields of carbon science, there should be many opportunities for new discoveries at the interface between these fields. Efforts to bridge the gap between workers in these sub-fields through joint symposia could be very fruitful.

As I look back upon my own career in carbon science, it has been unusually rewarding and filled with excitement. For over three decades our group has been involved in research covering a sufficiently broad spectrum of topics, so that it

has been possible for me to watch the field as a whole grow, prosper, and mature. Though much has been accomplished since 1961, when I entered the field, whenever I look at the carbon phase diagram I am reminded of the vast areas remaining to be discovered and explored. These intellectually challenging research frontiers and the promise of benefits to society from applications of previously acquired knowledge about carbon science keep me feeling young and excited about starting each new day.

ACKNOWLEDGMENTS

I would like to thank all of my many colleagues and students who have helped me over the years to discover the wonders of carbon science: Gene Dresselhaus, Morinobu Endo, Peter Eklund, Jean-Paul Issi, Riichiro Saito, Toshiaki Enoki, Radi A Jishi, AM Rao, Joseph Heremans, Joel McClure, John Mavroides, Jin-Joo Song, Deborah Chung, Steve Leung, Ko Sugihara, T Venkatesan, John Steinbeck, Gabriel Braunstein, Ian Spain, Harris Goldberg, Stan di Vittorio, Alex Fung, Sumio Iijima, Rick Pekala, Boris Elman, James Speck, Lourdes Salamanca-Riba, Paul Schroeder, Nai-Chang Yeh, Charles Olk, Joey Wang, Sei-ichi Tanuma, Rafi Kalish, Steven Praver, and many others. Support for this work has come from National Science Foundation grant No. DMR95-10093 and from subcontract B287707 from the US Department of Energy by Lawrence Livermore National Laboratory under Contract No. W-7405-ENG-48.

Visit the *Annual Reviews* home page at
<http://www.annurev.org>.

Literature Cited

1. Bundy FP. 1980. *J. Geophys. Res.* 85:6930
2. Bundy FP. 1985. In *Solid State Physics under Pressure: Recent Advances with Anvil Devices*, ed. S Minomura, p. 1. Dordrecht: Reidel
3. Moore AW, Ubbelohde AR, Young DA. 1962. *Brit. J. Appl. Phys.* 13:393
4. Kroto HW, Heath JR, O'Brien SC, Curl RF, Smalley RE. 1985. *Nature* 318:162-63
5. Iijima S. 1991. *Nature* 354:56
6. Bundy FP, Bassett WA, Weathers MS, Hemley RJ, Mao HK, Goncharov AF. 1996. *Carbon* 34:141-53
7. Bundy PP, Bovenkerk, HP, Strong RM, Wentorf RH Jr. 1961. *J. Chem. Phys.* 35:383
8. Bundy FP. 1963. *J. Chem. Phys.* 38:618
9. Whittaker AG, Kintner PL. 1969. *Science* 165:589
10. Whittaker AG. 1978. *Science* 200:763
11. Whittaker AG, Watts EJ, Lewis RS, Anders E. 1980. *Science* 209:1512
12. Whittaker AG, Kintner PL. 1985. *Carbon* 23:255
13. Kasatochkin VI, Sladkov AM, Kudryavtsev YP, Popov NM, Korshak VV. 1967. *Dokl. Chem.* 177:1031
14. Kasatochkin VI, Kasakov ME, Savransky VA, Nabatnikov AP, Radimov NP. 1971. *Dokl. Akad. Nauk.* 201:1104
15. Kasatochkin VI, Korshak VV, Kudryavtsev YP, Sladkov AM, Sterenberg IE. 1973. *Carbon* 11:70
16. El Goresy A, Donnay G. 1968. *Science* 161:363
17. Tanuma SI, Palnichenko A. 1995. *J. Mater. Res.* 10:1120
18. Palnichenko A, Tanuma SI. 1996. *J. Phys. Chem. Solids* 57:1163

19. Lettington A, Steeds JW, eds. 1994. *Thin Film Diamond*. London: Chapman & Hall
20. Dresselhaus MS, Dresselhaus G, Eklund PC. 1996. *Science of Fullerenes and Carbon Nanotubes*. New York: Academic
21. Kelly BT. 1981. *Physics of Graphite*. London: Applied Science. 472 pp.
22. Dresselhaus MS, Dresselhaus G, Sughara K, Spain IL, Goldberg HA. 1988. *Graphite Fibres and Filaments, Springer Series in Materials Science*. Berlin: Springer-Verlag. Vol. 5
23. Nakada K, Fujita M, Dresselhaus G, Dresselhaus MS. 1996. *Phys. Rev. B* 54:17954
24. McClure JW. 1956. *Phys. Rev.* 104:666
25. Sato K, Noguchi M, Demachi A, Oki N, Endo M. 1994. *Science* 264:556
26. Matthews MJ, Dresselhaus MS, Endo M, Sasabe Y, Takahashi T, Takeuchi K. 1996. *J. Mater. Res.* 11:3099
27. Dresselhaus MS, Dresselhaus G. 1981. *Adv. Phys.* 30:139–326
28. Nakadaira M, Saito R, Kimura T, Dresselhaus G, Dresselhaus MS. 1997. *J. Mater. Res.* In press
29. Heimann RB, Kleiman J, Slansky NM. 1983. *Nature* 306:164
30. Zabel H, Solin SA, eds. 1990. *Graphite Intercalation Compounds I. Structure and Dynamics*. Berlin: Springer-Verlag. Vol. 14
31. Rüdorff W, Shultze E. 1954. *Z. Anorg. allg. Chem.* 277:156
32. Matsubara K, Tsuzuku T, Murakami M. 1991. *20th Biennial Conf. Carbon, Santa Barbara, Ext. Abst.* p. 556
33. Yasujima H, Murakami M, Yoshimura S. 1986. *Appl. Phys. Lett.* 49:499
34. Hishiyama Y, Yasuda S, Inagaki M. 1988. *J. Mater. Sci.* 23:3722
35. Inagaki M, Harada S, Sato T, Nakajima T, Horino Y, Morata K. 1988. *Carbon* 27:253
36. Hishiyama Y, Kaburagi Y, Inagaki M. 1991. In *Chemistry and Physics of Carbon*, ed. PA Thrower, 23:1. New York: Dekker
37. Krätschmer W, Fostiropoulos K, Huffman DR. 1989. In *Dusty Objects in the Universe; Proc. 4th Int. Workshop Astronomical Observatory of Capodimonte, Capri, Italy*, ed. E Bussoletti, AA Vittono. Dordrecht: Kluwer
38. Gamaly EG, Ebbesen TW. 1995. *Phys. Rev. B* 52:2083
39. Kaiser M, Maser WK, Byrne HJ, Mittelbach A, Roth S. 1993. *Solid State Commun.* 87:281–84
40. Könenkamp R, Erxmeyer J, Weldinger A. 1994. *Appl. Phys. Lett.* 65:758–60
41. Kazaoui S, Ross R, Minami N. 1994. *Solid State Commun.* 90:623–28
42. Rao AM, Zhou P, Wang K-A, Hager GT, Holden JM, et al. 1993. *Science* 259:955–57
43. Hebard AF, Eom CB, Fleming RM, Chabal YJ, Muller AJ, et al. 1993. *Appl. Phys. A* 57:299–303
44. Wang Y, Holden JM, Dong ZH, Bi XX, Eklund PC. 1993. *Chem. Phys. Lett.* 211:341
45. Fleischer SB, Pevzner B, Dougherty DJ, Ippen EP, Dresselhaus MS, Hebard AF. 1996. *Appl. Phys. Lett.* 69:296–98
46. Taylor R, Walton DRM. 1993. *Nature* 363:685
47. Hamza AV, Balooch M, Moalem M. 1994. *Surf. Sci.* 317:L1129–35
48. Viitanen J. 1993. *J. Vacuum Sci. Tech. B. Microelectron. Proc. Phenom.* 11:115–16
49. Devel M, Girard C, Joachim C, Martin OJF. 1995. *Appl. Surf. Sci.* 87–88:390–97
50. Bethune DS, Johnson RD, Salem JR, de Vries MS, Yannoni CS. 1993. *Nature* 366:123
51. Saito S, Sawada S, Hamada N. 1992. *Phys. Rev. B* 45:13845
52. Nagase S, Kobayashi K. 1994. *Chem. Phys. Lett.* 228:106–10
53. Poirier DM, Knupfer M, Weaver JH, Andreoni W, Laasonen K, et al. 1994. *Phys. Rev. B* 49:17403
54. Wästberg B, Rosén A. 1991. *Phys. Scr.* 44:276
55. Chang AHH, Ermler WC, Pitzer RM. 1991. *J. Chem. Phys.* 94:5004
56. Zimmermann U, Malinowski N, Näher U, Frank S, Martin TP. 1994. *Phys. Rev. Lett.* 72:3542
57. Martin TP, Malinowski N, Zimmermann U, Näher U, Schaber H. 1993. *J. Chem. Phys.* 99:4210
58. Kohanoff J, Andreoni W, Parrinello M. 1992. *Chem. Phys. Lett.* 198:472
59. Iijima S, Ichihashi T. 1993. *Nature* 363:603
60. Bethune DS, Kiang CH, de Vries MS, Gorman G, Savoy R, et al. 1993. *Nature* 363:605
61. Thess A, Lee R, Nikolaev P, Dai H, Petit P, et al. 1996. *Science* 273:483
62. Endo M. 1975. *Mecanisme de croissance en phase vapeur de fibres de carbone*. PhD thesis, Univ. Orleans, Orleans, France (in French) 165 pp.
63. Endo M, Koyama T, Hishiyama Y. 1976. *Jpn. J. Appl. Phys.* 15:2073–76
64. Dresselhaus MS, Dresselhaus G, Saito R. 1995. *Carbon* 33:883–91

65. Saito R, Fujita M, Dresselhaus G, Dresselhaus MS. 1992. *Appl. Phys. Lett.* 60:2204
66. Painter GS, Ellis DE. 1970. *Phys. Rev. B* 1:4747
67. Olk CH, Heremans JP. 1994. *J. Mater. Res.* 9:259
68. Dresselhaus MS. 1996. *Phys. World*, p. 18
69. Saito R, Dresselhaus G, Dresselhaus MS. 1996. *Phys. Rev. B* 53:2044
70. Chico L, Crespi VH, Benedict LX, Louie SG, Cohen ML. 1996. *Phys. Rev. Lett.* 76:971
71. Lambin Ph, Fonseca A, Vigneron JP, Nagy JB, Lucas AA. 1995. *Chem. Phys. Lett.* 245:85
72. Saito Y. 1995. *Carbon* 33:979
73. Saito Y, Yoshikawa T, Okuda M, Ohkohchi M, Ando Y, et al. 1994. *Chem. Phys. Lett.* 209:72
74. Ugarte D. 1992. *Nature* 359:707
75. Ugarte D. 1993. *Chem. Phys. Lett.* 207:473
76. Ugarte D. 1995. *Carbon* 33:989
77. Kroto H. 1992. *Nature* 359:670
78. Ugarte D. 1993. *Europhys. Lett.* 22:45
79. Yamada K, Kunishige H, Sowaoka AB. 1991. *Naturwissenschaften* 78:450
80. Hatta N, Murata K. 1994. *Chem. Phys. Lett.* 217:398
81. Weathers LS, Basset WA. 1987. *Phys. Chem. Min.* 15:105
82. Kuznetsov VL, Chuvilin AL, Butenko YV, Mal'kov IY, Titov VM. 1994. *Chem. Phys. Lett.* 222:343
83. Speck JS. 1990. *J. Appl. Phys.* 67:495
84. Maiti A, Bravbec J, Bernholc J. 1993. *Phys. Rev. Lett.* 70:3023
85. Tomanek D, Zhong W, Kravest E. 1993. *Phys. Rev. B* 48:15461
86. Tuinstra F, Koenig JL. 1970. *J. Chem. Phys.* 53:1126
87. Fourdeux A, Perret R, Ruland W. 1971. *Int. Conf. Carbon Fibers and Their Composites*, p. 57. The Plastics Institute
88. Bokros JC. 1969. In *Chemistry and Physics of Carbon*, ed. PL Walker, Jr. 5:1. New York: Dekker
89. Matthews MJ, Dresselhaus MS, Dresselhaus G, Endo M, Nishimura Y, et al. 1996. *Appl. Phys. Lett.* 69:430-32
90. Endo M, Takeuchi K, Kobori K, Takahashi K, Kroto H, Sarkar A. 1995. *Carbon* 33:873
91. Endo M, Takeuchi K, Hiraoka T, Furuta T, Kasai T, Sun X, et al. 1996. *Proc. Int. Conf. Fullerenes, Oxford, UK*
92. Dahn JR. 1991. *Phys. Rev. B* 44:9170
93. Wilson AM, Way BM, Dahn JR. 1995. *J. Appl. Phys.* 77:2363
94. Conard J, Nalimova VA, Guerard D. 1994. *Mol. Cryst. Liq. Cryst.* 245:25-30
95. Megahed S, Scrosati B. 1994. *J. Power Sources* 51:79
96. Matthews MJ, Bi XX, Dresselhaus MS, Endo M, Takahashi T. 1996. *Appl. Phys. Lett.* 68:1078-80
97. Matthews MJ, Dresselhaus MS, Kobayashi N, Enoki T, Endo M, Takahashi T. 1996. *Appl. Phys. Lett.* 69:2042-44
98. Dresselhaus MS, Fung AWP, Rao AM, di Vittorio SL, Kuriyama K, et al. 1992. *Carbon* 30:1065-73
99. Pekala RW, Alviso CT. 1992. In *Novel Forms of Carbon*, ed. CL Renschler, JJ Pouch, DM Cox. 270:3-14. Pittsburgh, PA: Mater. Res. Soc.
100. Fung AWP, Wang ZH, Lu K, Dresselhaus MS, Pekala RW. 1993. *J. Mater. Res.* 8:1875